Applied Catalysis B: Environmental 180 (2016) 20–28

Contents lists available at ScienceDirect

Applied Catalysis B: Environmental

journal homepage: www.elsevier.com/locate/apcatb

Synergistic photocatalytic properties and mechanism of g-C_3N_4 coupled with zinc phthalocyanine catalyst under visible light irradiation

Wangyang Lu*, Tiefeng Xu, Yu Wang, Hongguang Hu, Nan Li, Xuemei Jiang, Wenxing Chen*

National Engineering Lab for Textile Fiber Materials & Processing Technology (Zhejiang), Zhejiang Sci-Tech University, Hangzhou 310018, China

ARTICLE INFO

Article history:
Received 11 March 2015
Received in revised form 1 June 2015
Accepted 5 June 2015
Available online 9 June 2015

Keywords:
G-C_3N_4
Zinc phthalocyanine
Visible light
Mechanism
Degradation pathway

ABSTRACT

Visible light-responsive photocatalysis has shown great potential for effluent treatment as an environmentally friendly method. Herein, the photocatalyst of graphitic carbon nitride (g-C_3N_4) coupled with zinc phthalocyanine (g-C_3N_4/ZnTcPc) was prepared by immobilizing zinc tetracarboxyphthalocyanine (ZnTcPc) onto g-C_3N_4 covalently. The spectral response region of g-C_3N_4 has been extended from 450 nm to more than 800 nm sensitized by ZnTcPc, which is well known for the red/near-IR (Q band) light absorption. Compared with pure g-C_3N_4 and ZnTcPc, g-C_3N_4/ZnTcPc presented a significantly enhanced photocatalytic activity for the degradation of rhodamine B (RhB) and 4-chlorophenol (4-CP) under visible irradiation. The photocatalytic activity of g-C_3N_4 has been improved by the coupled interaction with ZnTcPc over a wide pH range. Moreover, besides photogenerated hole, the presence of singlet oxygen ($^1O_2$), superoxide radical ($^{\bullet}O_2^-$) and hydroxyl radical ($^{\bullet}OH$) has been evidenced in the visible light-responsive catalytic system with g-C_3N_4/ZnTcPc, especially in alkaline condition. The possible photocatalytic degradation pathway of RhB has been proposed according to the results of ultra-performance liquid chromatography and high-definition mass spectrometry (UPLC Synapt G2-S HDMS). This synergistic photocatalytic process will provide useful insights to make full use of solar light for future application to eliminate recalcitrant organic pollutants.

1. Introduction

Photocatalysis for the degradation of organic pollutants has gained increasing attention as a promising technique [1–3]. A large amount of photocatalytic materials have been investigated, including TiO_2 [4–6], ZnO [7,8], CdS [9,10], g-C_3N_4 [11,12], etc. Among the reported photocatalytic materials, g-C_3N_4 as a novel metal-free polymeric photocatalyst has good photocatalytic performance under visible light irradiation [13,14], and it also demonstrates the property of low cost, non-toxicity, and thermal stability [15]. Therefore, g-C_3N_4 has been widely used in the degradation of organic pollutants [13,14] and the direct production of clean hydrogen [11,16,17]. However, the position of absorption edge of g-C_3N_4 is around 450 nm with a band gap of 2.7 eV, which restricts its utilization under visible light irradiation [18]. Hence, there is a need to develop an efficient visible light responsive photocatalyst to extend its spectral response to higher absorption wavelength.

A lot of attempts have been made to improve the visible light response of g-C_3N_4 based photocatalysts, such as the synthesis of heterojunction composite photocatalysts [19–21] and dye-sensitization [22]. As an effective photosensitizer, zinc porphyrin has been employed to sensitize photocatalytic materials to extend the absorption spectra [23]. Moreover, some studies suggested that porphyrin with carboxyl group is helpful for electron transfer from excited-state of porphyrin sensitizer to the conduction band of semiconductor materials [24,25]. In our previous study, zinc phthalocyanine (ZnPc) and its derivatives possess a wide visible light response (600 ~ 800 nm) [26–28]. They can be synthesized with different substituent groups and combined with other compounds by loading or coordination. The synthetic flexibility of phthalocyanines offers great possibilities to modify the length of the connection groups and the positions of substituted groups [29]. Furthermore, ZnPc is able to photochemically activate triplet oxygen into singlet oxygen ($^1O_2$), which is frequently used as a non-radical oxidant for oxidizing organic

* Corresponding authors. Fax: +86 571 86843611.
E-mail addresses: luwy@zstu.edu.cn (W. Lu), wxchen@zstu.edu.cn (W. Chen).

http://dx.doi.org/10.1016/j.apcatb.2015.06.009
0926-3373/

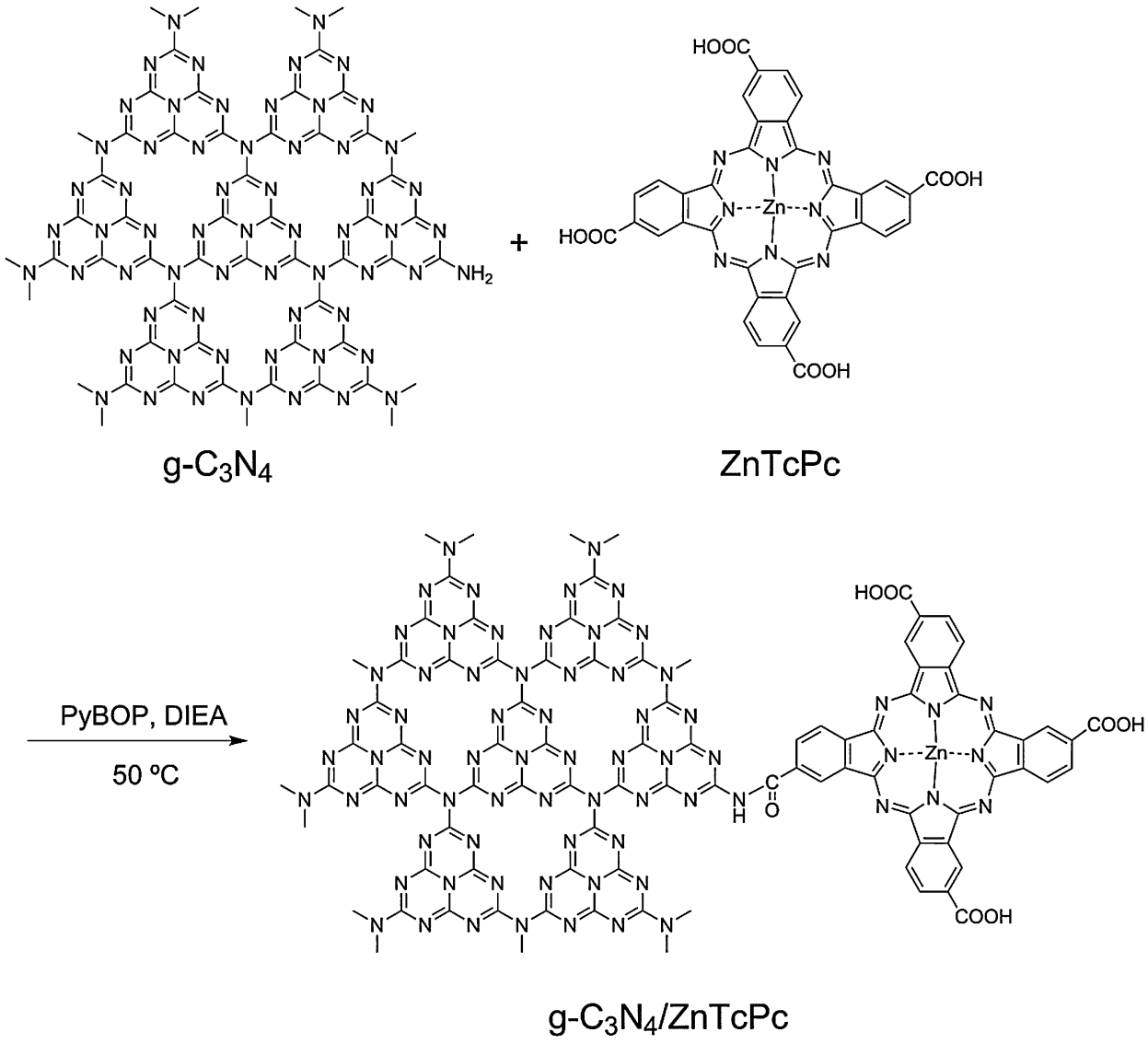

Scheme 1. Synthesis of g-C_3N_4/ZnTcPc.

pollutants [30]. Therefore, combining the photoresponsive property of both g-C_3N_4 and ZnPc to prepare a photocatalyst with the extended spectral response in the whole visible wavelength range and higher photocatalytic activity seems to be extraordinarily vital.

In this paper, g-C_3N_4 coupled with zinc phthalocyanine (g-C_3N_4/ZnTcPc) catalyst was prepared by immobilizing zinc tetracarboxyphthalocyanine (ZnTcPc) onto g-C_3N_4 covalently. Rhodamine B (RhB) and 4-chlorophenol (4-CP) were used to evaluate the photocatalytic activities of g-C_3N_4/ZnTcPc under visible light irradiation, and the effect of the ZnTcPc amounts and pH were also investigated. The results showed that g-C_3N_4/ZnTcPc showed higher photocatalytic activity and such good photocatalytic property could maintain at a high level in a wider pH range. Furthermore, some typical scavengers were added to identify the active species in the photocatalytic oxidation process, and the possible synergistic photocatalytic mechanism was proposed. Finally, the possible degradation pathway of RhB was discussed based on the intermediates analyzed by ultra-performance liquid chromatography (UPLC) and high-definition mass spectrometry (HDMS).

2. Experimental

2.1. Materials and reagents

RhB and 4-CP were purchased from Tokyo Chemical Industry Co., Ltd., Benzotriazol-1-yl-oxytripyrrolidinophosphonium hexafluorophosphate (PyBOP), *N*,*N*-diisopropylethylamine (DIEA), and p-benzoquinone (BQ) were purchased from Aladdin Chemical Co., Ltd., Isopropanol (IPA) and potassium iodide (KI) were obtained from Tianjin Wing Tai Chemical Co., Ltd., and Hangzhou Gao Jing Fine Chemical Co., Ltd., respectively. Acetonitrile and methanol (Merck, Germany) were chromatographic grade for UPLC. All other chemicals were analytical grade and were used without further purification. The water used in all experiments was ultrapure water from Milli-Q Advantage A10 (Millipore).

2.2. Preparation of g-C_3N_4/ZnTcPc

g-C_3N_4 was prepared by the thermal decomposition of urea [31]. 30 g urea in a covered crucible was heated to 550 °C in a tune furnace at a heating rate of 2.5 °C/min, and then retained at 550 °C

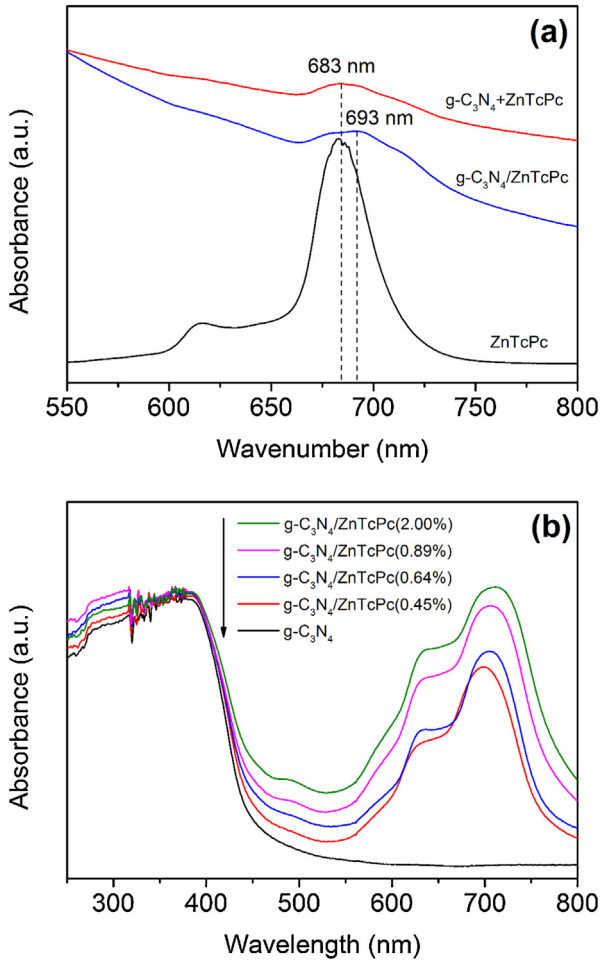

Fig. 1. (a) UV–vis spectra of ZnTcPc, g-C_3N_4/ZnTcPc(0.64%) and g-C_3N_4 + ZnTcPc (0.64%) solution; (b) UV–vis diffuse reflectance absorption spectrum of g-C_3N_4, g-C_3N_4/ZnTcPc(0.45%), g-C_3N_4/ZnTcPc(0.64%), g-C_3N_4/ZnTcPc(0.89%) and g-C_3N_4/ZnTcPc (2.00%).

for 3 h. After cooling, the resultant pale yellow powder was collected. ZnTcPc was synthesized according to the literature [32]. Scheme 1 shows the preparation process of g-C_3N_4/ZnTcPc. g-C_3N_4 was dispersed in DMF, and then ultrasounded for 20 h. The ZnTcPc, PyBOP and DIEA (with the molar ratio of 1:2:4) were dissolved in 100 mL DMF and ultrasounded for 5 h. The ultrasonic g-C_3N_4 dispersion was added dropwise to the ZnTcPc solution at a rate of 100 mL/h. After reacting for 6 h, the solution was filtered, washed with DMF, 1 mol/L NaOH solution, ultrapure water, respectively, and freeze-dried to obtain g-C_3N_4/ZnTcPc catalyst. A series of g-C_3N_4/ZnTcPc catalysts with different mass ratios of ZnTcPc were prepared. According to the results of inductively coupled plasma spectroscopy (ICP) test, the content of zinc is shown as Fig. S1, then the concentration of ZnTcPc was calculated by the following equation,

$$W = \frac{11.75CV}{1000m} \quad (1)$$

where, C is the concentration of the sample (mg/L), V is the volume of the sample solution (L), m is the mass of sample, and W is the mass fraction of ZnTcPc in the g-C_3N_4/ZnTcPc catalyst. The as-prepared photocatalysts were named as g-C_3N_4/ZnTcPc (0.45%), g-C_3N_4/ZnTcPc (0.64%), g-C_3N_4/ZnTcPc (0.89%), g-C_3N_4/ZnTcPc (2.00%), respectively. And the mixture of g-C_3N_4 and ZnTcPc was defined as g-C_3N_4 + ZnTcPc (0.64% ZnTcPc in the mixture).

2.3. Characterization

Transmission electron microscope (TEM) was operated at a JEM-2010 transmission electron microscope (JEOL, Japan). X-ray diffraction (XRD) spectroscopy of the samples were recorded by a DX-2700 X-ray diffractometer (Dandong Fangyuan, China) with Cu–Kα radiation at 2θ angles ranging from 5 to 50° at a rate of 3°/min. The UV–vis diffuse reflection spectra were recorded at a Lambda 900 UV–vis spectrometer (Perkin Elmer, USA). The UV–vis spectrometer (UV-2550, Shimadzu, Japan) was used to investigate the optical absorption properties of the samples. Thermogravimetric analysis (TGA) was carried out on TGA 1 (Mettler Toledo, Switzerland) from 25 to 800 °C at a heating rate of 10 °C/min. X-ray photoelectron spectroscopy (XPS) was measured on a Thermo Scientific K-Alpha spectrometer (monochromatic Al Kα, 1486.6 eV).

2.4. Photocatalytic experiments

The photocatalytic performance of g-C_3N_4/ZnTcPc was conducted in a glass sample beaker with side irradiation provided by a 100 W lamp (LOT-oriel GmbH & Co., KG). A UV cutoff filter (Shanghai Seagull Colored Optical Glass Co., Ltd.) was employed to filter the UV light (λ < 400 nm) to ensure illumination by visible light only. g-C_3N_4/ZnTcPc (0.1 g/L) was dispersed in RhB aqueous solution (2×10^{-5} mol/L) and the photocatalytic experiment was carried out at ambient temperature and atmospheric pressure. The distance between the lamp and reactor containing RhB solution was about 22 cm. Before irradiation, the suspension was treated by ultrasonication for dispersion uniformity. At given time intervals, the solution was continually taken from the reactor and filtered. The concentration of RhB was determined by UV–vis spectrometer at 554 nm. The pH of the reaction system was adjusted by the addition of H_2SO_4 or NaOH.

The transient photocurrent response was performed on an electrochemical analyzer (CHI660E, China) by a 671 nm laser or a 100 W lamp (λ > 400 nm) as a light source. The prepared photocatalyst film electrodes on carbon paper served as the working electrodes. The working electrodes were prepared as follows: 2 mg catalyst was added into the mixed solution of ultrapure water, isopropanol and perfluorosulfonic acid polymer (Nafion), then the obtained slurry was dip-coated onto the surface of the carbon paper with a size of 1 × 5 cm and dried at 60 °C. A Pt wire served as the counter electrode and Ag/AgCl (saturated KCl) served as a reference electrode.

2.5. Analytical methods

The intermediates formed during the RhB degradation photocatalyzed by g-C_3N_4/ZnTcPc were identified using UPLC Synapt G2-S HDMS (Waters, USA) with an electrospray ionization (ESI) source. The ion mode was set both on positive and negative mode. In the positive mode, the MS conditions were as follows: capillary voltage 3 kV, cone voltage 40 V, source temperature 120 °C, and desolvation temperature 400 °C. High purity nitrogen gas was used as both cone and desolvation gases at a flow rate of 50 and 900 L/h, respectively. Chromatographic separation was conducted with a BEH C18 column (1.7 μm, 2.1 × 100 mm) using mobile phases A (water) and B (acetonitrile). The eluent gradient began with 60% A at 0 min, where it was held for 1.0 min, followed by a decrease to 30% A at 7 min, and in the next 1 min it remained at 10% A, finally reaching 60% A at 8.1 min. The flow rate was 0.4 mL/min, and the column oven temperature was set at 30 °C. 8 μL sample solution was injected using the auto sampler. In the negative mode, the final degradation solution was freeze-dried, and the conditions were as follows: capillary voltage 2.5 kV, source temperature 150 °C, and desolvation temperature 500 °C. High purity

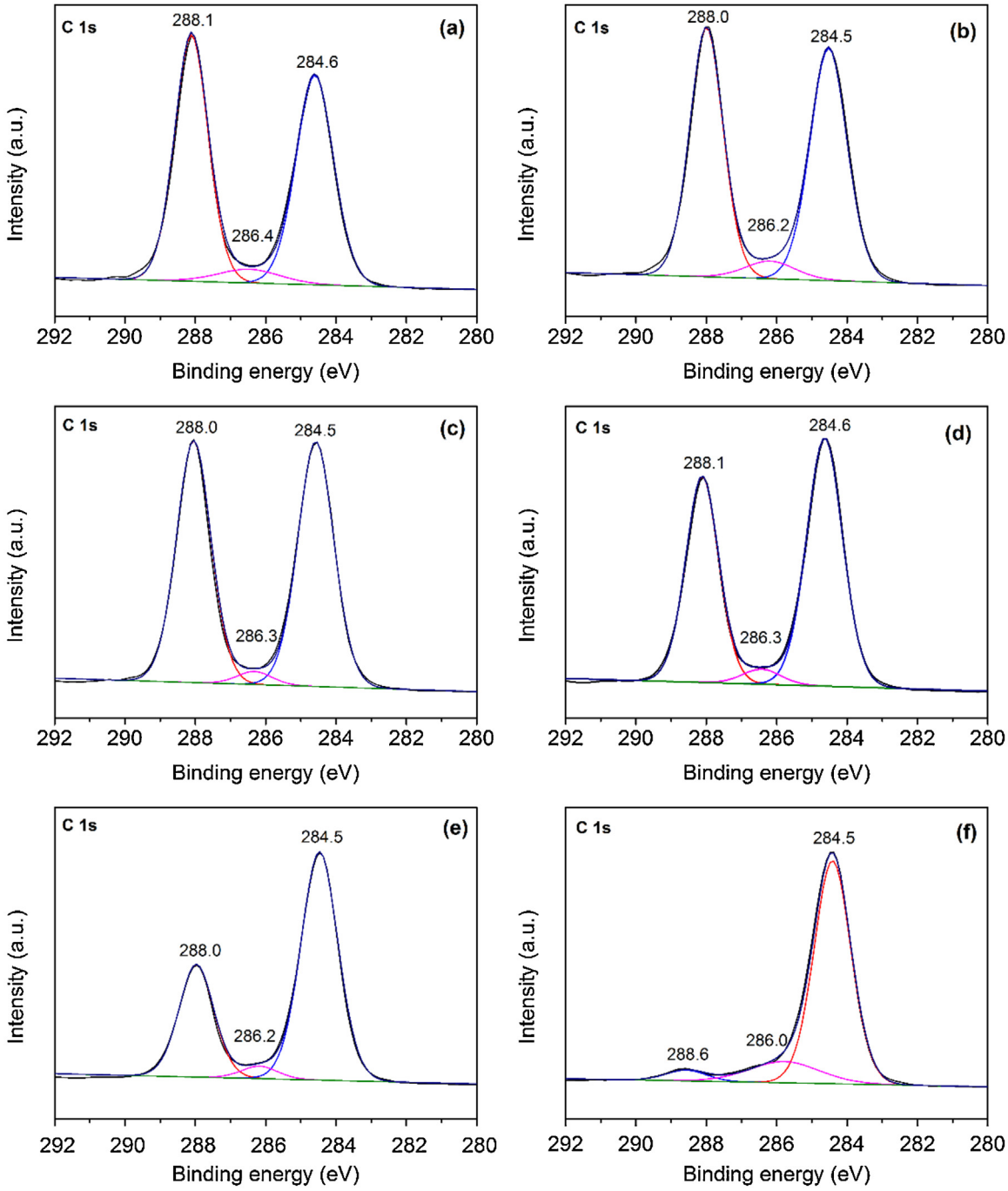

Fig. 2. Curve fit of the C 1s peak of (a) g-C_3N_4, (b) g-C_3N_4/ZnTcPc(0.45%), (c) g-C_3N_4/ZnTcPc(0.64%), (d) g-C_3N_4/ZnTcPc(0.89%), (e) g-C_3N_4/ZnTcPc(2.00%) and (f) ZnTcPc.

nitrogen gas was used as both cone and desolvation gases at a flow rate of 50 and 800 L/h, respectively. Chromatographic separation was conducted with a HSS T3 column (1.8 μm, 2.1 × 100 mm) using mobile phases A (water) and B (acetonitrile). The gradient began with 95% A at 0 min, where it was held for 0.5 min, followed by a decrease to 80% A at 5 min. The gradient reached 50% A at 7 min, and in the next 1 min it remained at 10% A, finally reaching 95% A at 9.1 min. The flow rate was 0.3 mL/min, and the column oven temperature was set at 30 °C. 2 μL solution was injected using the auto sampler. The parameters for UPLC Synapt G2-S HDMS analyses were as follow: ESI ion mode, lockmass correction of leucine enkephaline (LE, Tyr-Gly-Gly-Phe-Leu, negative *m*/*z* 554.2615, positive *m*/*z* 556.2771), and the scan range was set to 50–1200 *m*/*z*.

3. Results and discussion

3.1. Characterization

As shown in Fig. 1a, the UV–vis spectra of ZnTcPc shows a good absorption on the wavelength of light about 683 nm. The absorption of the simple mixture of g-C_3N_4 and ZnTcPc around 683 nm originates from the absorption of ZnTcPc. Compared with the mixture catalyst g-C_3N_4 + ZnTcPc, the absorption of g-C_3N_4/ZnTcPc is red-shifted about 10 nm. This result indicated that the bonding between g-C_3N_4 and ZnTcPc occurred to form an amide bond. In addition, the pure g-C_3N_4 only has a good absorption on the wavelength of light less than 450 nm (Fig. 1b). g-C_3N_4/ZnTcPc shows much broader absorption band through the entire visible light region. It

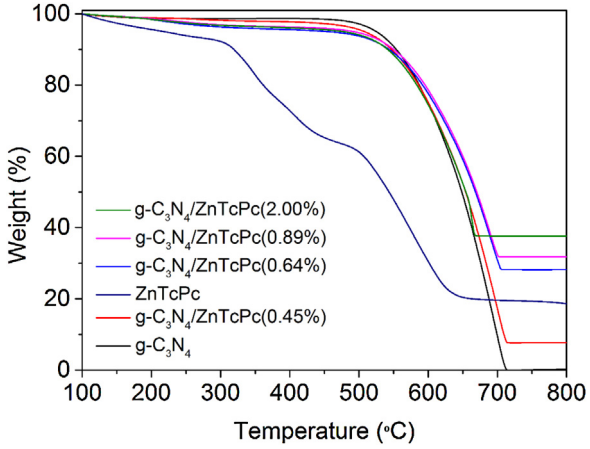

Fig. 3. Thermogravimetric analysis for g-C_3N_4, g-C_3N_4/ZnTcPc(0.45%), g-C_3N_4/ZnTcPc(0.64%), g-C_3N_4/ZnTcPc(0.89%), g-C_3N_4/ZnTcPc(2.00%) and ZnTcPc.

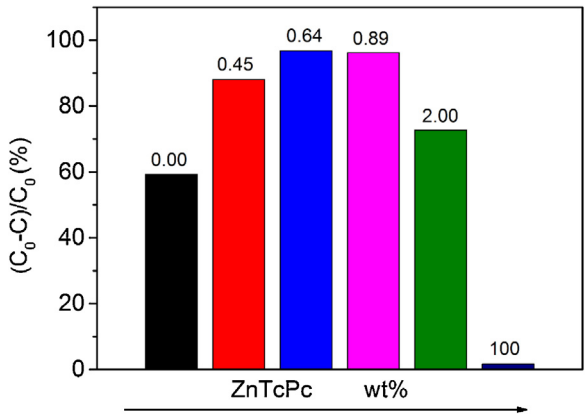

Fig. 4. The removal rate for the photodegradation of RhB (2×10^{-5} mol/L) over g-C_3N_4/ZnTcPc with different grafting amounts of ZnTcPc under visible light irradiation ($\lambda > 400$ nm) for 90 min. [ZnTcPc] = 0.1 g/L, pH 9.

reaches the maximum absorption peak at around 700 nm. All g-C_3N_4/ZnTcPc photocatalysts exhibit intense and excellent visible light absorption properties. Moreover, the spectral absorption of g-C_3N_4/ZnTcPc at around 700 nm can be obviously enhanced with the increasing amount of ZnTcPc in g-C_3N_4/ZnTcPc. Based on the above observations and discussion, it could be concluded that the strong conjugated interaction between g-C_3N_4 and ZnTcPc might induce a synergetic effect for enhancing the photoactivity of g-C_3N_4 and ZnTcPc.

We used XPS spectra to further prove, the conjugated interaction between g-C_3N_4 and ZnTcPc. The deconvoluted XPS spectra of C 1s, N 1s and Zn 2p reveal the chemical character of C, N and Zn, respectively, for g-C_3N_4, ZnTcPc, g-C_3N_4/ZnTcPc. It can been seen that the C 1s peaks at 284.5–284.6, 286.0–286.4 and 288.0–288.06 eV are attributed to C—C, C—NH_2 and N—C=N, respectively (Fig. 2) [33–35]. With the increasing amount of ZnTcPc, the N—C=N peak of g-C_3N_4/ZnTcPc is declined compared with the C—C peak. This might be due to the amidation reaction between g-C_3N_4 and ZnTcPc, decreasing the amount of N—C=N bond. According to the N 1s peaks in Fig. S2, we can observe that the N 1s peak of g-C_3N_4 at 398.5 eV is attributed to the triazine rings, and the N 1s peak of ZnTcPc occurring at 398.5 eV is due to aza-bridging and pyrrole nitrogen atoms [36,37]. Besides, the increasing peak at 401.1 eV based on g-C_3N_4/ZnTcPc may be explained by the nitrogen of the amide group (—NH—CO—), which was formed for the bonding between the amino (—NH_2) and substituted carboxyl groups (Fig. S2b and e). Therefore, we conclude that ZnTcPc was immobilized on g-C_3N_4 by amide linkage. The Zn 2p features were also examined. Because of the low amount, it did not show any apparent characteristic, except for the Zn $2p_{3/2}$ and Zn $2p_{1/2}$ peaks of g-C_3N_4/ZnTcPc (2.00%) at 1021.8 and 1044.7 eV (Fig. S3) [38]. The above results indicated that ZnTcPc has been immobilized on g-C_3N_4 covalently.

Moreover, the TG technique was employed to verify the thermal stability of g-C_3N_4/ZnTcPc. As observed in the TG curve in Fig. 3, pure g-C_3N_4 has good thermal stability and its decomposition temperature is above 500 °C. However, when it is held at 720 °C, it can be eliminated completely and there is no residual carbon left. As for pure ZnTcPc, there are mainly three weight-loss steps on the curve of TG and its total weight loss is about 80%. With the increasing content of ZnTcPc, g-C_3N_4/ZnTcPc exhibits more stable when the temperature is above 720 °C. The weight loss from 200 °C to 500 °C can be related to the decomposition of the peripheral substituents in ZnTcPc, finally forming some stable compounds to covering g-C_3N_4 and improving the thermal stability of g-C_3N_4.

X-ray diffraction patterns (XRD) was used to identify the phase structures of the as-prepared samples. As shown in Fig. S4, two distinct peaks at 13.1 and 27.5° for pure g-C_3N_4 can be indexed, respectively. The stronger one at 27.5° can be indexed as (0 0 2) diffraction for graphitic materials. The interlayer D-spacing corresponds well to that of g-C_3N_4 (0.324 nm). The diffraction peak at 13.1° corresponds to an interplanar separation of 0.682 nm and is indexed as (1 0 0) in JCPDS 87-1526 [14]. This result provided that the covalent structure of g-C_3N_4/ZnTcPc did not change the crystal structure of g-C_3N_4. Besides, it can be seen from TEM images that the introduction of ZnTcPc has no effect on the layer structure of g-C_3N_4 (Fig. S5).

3.2. Photocatalytic activity

The photocatalytic activities of the as-prepared g-C_3N_4, ZnTcPc, g-C_3N_4/ZnTcPc and the mixture of g-C_3N_4 and ZnTcPc were evaluated by the degradation of RhB and 4-CP in aqueous solution under visible light irradiation. First, we studied the influence of the ZnTcPc amount in g-C_3N_4/ZnTcPc on the photocatalytic activity under the same conditions. As shown in Fig. 4, the removal rate of RhB using g-C_3N_4/ZnTcPc as the photocatalyst was higher than that of pure g-C_3N_4 or ZnTcPc, and it improved gradually with the increase of the ZnTcPc amount. When the percent of ZnTcPc reached 0.64%, it exhibited the highest photocatalytic activity. However, the photocatalytic activity of g-C_3N_4/ZnTcPc (2.00%) was significantly lower than that of g-C_3N_4/ZnTcPc (0.64%). The reason might be that the too strong absorption of ZnTcPc to visible light could weaken the absorption of visible light by g-C_3N_4, causing the decrease of photocatalytic activity. In the following studies, g-C_3N_4/ZnTcPc (0.64%) was chosen to investigate the performance of g-C_3N_4/ZnTcPc. As shown in Fig. 5, there was no obvious change in the concentration of RhB in the presence of ZnTcPc, suggesting that ZnTcPc had almost no photocatalytic activity for the degradation of RhB. In the presence of g-C_3N_4, the removal rate of RhB was about 58%. In addition, the mixture of g-C_3N_4 and ZnTcPc (g-C_3N_4+ZnTcPc) also showed a low photocatalytic performance with a removal rate of 68%. However, when g-C_3N_4/ZnTcPc was present, more than 98% of RhB was degraded, which was obviously higher than that of pure g-C_3N_4. Similarly, g-C_3N_4/ZnTcPc performed apparently higher photocatalytic activity on the degradation of 4-CP (Fig. S6) than g-C_3N_4 and ZnTcPc, which indicated that the degradation of RhB was not caused by the sensitization effect. And it can be explained by the results of the electron paramagnetic resonance. According to the above results, we inferred that the enhanced activities were due to the synergistic effect between g-C_3N_4 and ZnTcPc.

The pH value is a significant parameter in the degradation of organic pollutant in aqueous solution and the higher activity

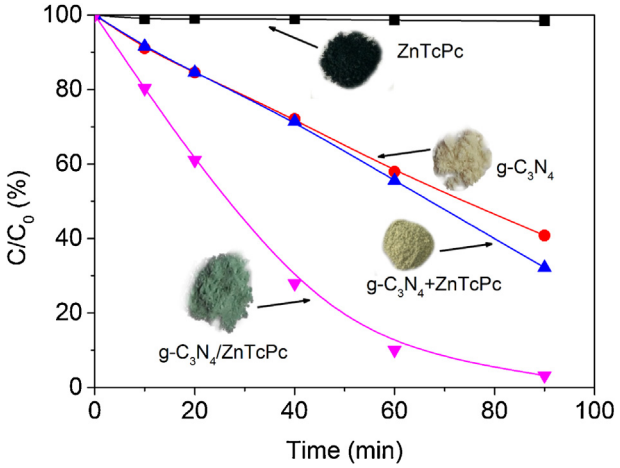

Fig. 5. Photocatalytic degradation of RhB (2×10^{-5} mol/L) in the presence of g-C_3N_4, g-C_3N_4 + ZnTcPc(0.64%), g-C_3N_4/ZnTcPc(0.64%) and ZnTcPc under visible light irradiation ($\lambda > 400$ nm). [g-C_3N_4] = 0.1 g/L, [g-C_3N_4 + ZnTcPc] = 0.1 g/L, [g-C_3N_4/ZnTcPc] = 0.1 g/L, pH 9 (The same content of ZnTcPc in three different systems.).

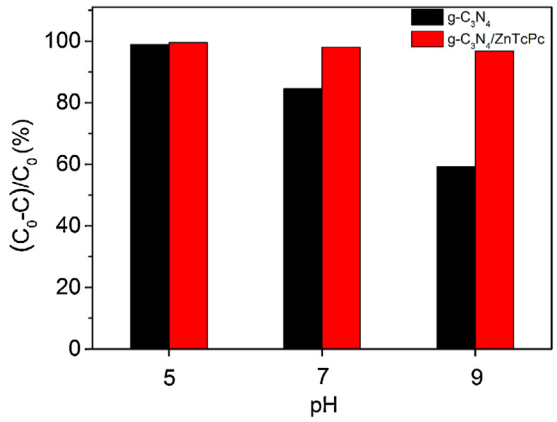

Fig. 6. The removal rate for the photocatalytic degradation of RhB (2×10^{-5} mol/L) at different pH in the presence of g-C_3N_4 and g-C_3N_4/ZnTcPc under visible light irradiation ($\lambda > 400$ nm). [g-C_3N_4] = 0.1 g/L, [g-C_3N_4/ZnTcPc(0.64%)] = 0.1 g/L.

usually occurred in acidic addition [39]. Here, the photocatalytic degradation processes of RhB with g-C_3N_4 and g-C_3N_4/ZnTcPc were studied under different pH conditions, as shown in Fig. 6. g-C_3N_4 showed a good photocatalytic activity under an acidic condition (pH 5), but exhibited very poor photocatalytic activity at pH 9. However, no matter under acidic, neutral and alkaline conditions, g-C_3N_4/ZnTcPc presented very high photocatalytic activity for the degradation of RhB. Therefore, compared with g-C_3N_4, g-C_3N_4/ZnTcPc showed higher photocatalytic activity over a wider pH range. More importantly, it suggested that the introduction of ZnTcPc might result in a different photocatalytic mechanism that was different with g-C_3N_4. This result is very significant for the treatment of the actual wastewater, because the practical effluents containing organic dyes and phenols from industries such as papermaking, bleaching and dyeing are typically alkaline [40]. Moreover, the regenerating performance is a key character of catalysts that to be usable in practice, thus the recycling experiments of g-C_3N_4/ZnTcPc were carried out (Fig. S7). After repeating this experiment ten times, the removal rate was as high as 99% and had no obvious decrease, indicating that g-C_3N_4/ZnTcPc has broad application prospect for removing organics.

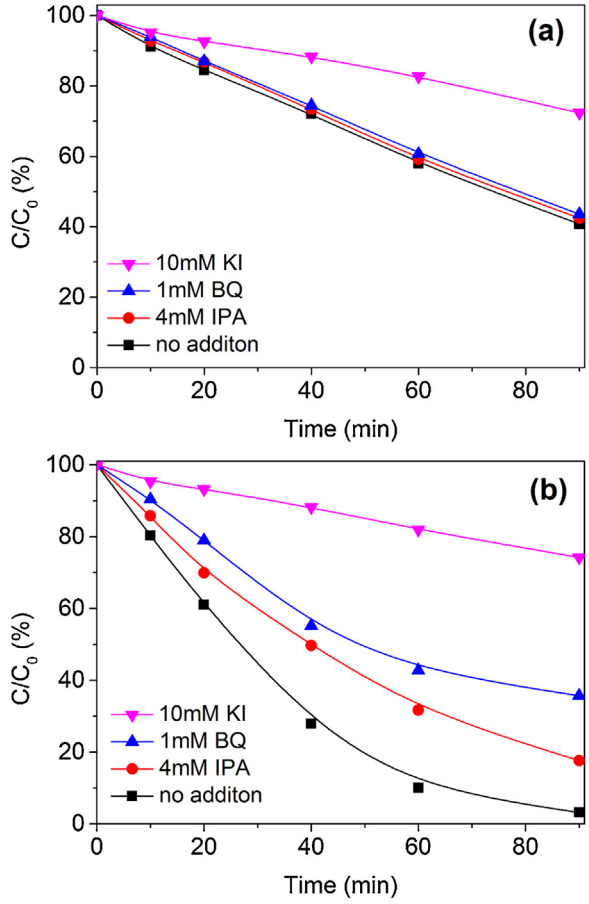

Fig. 7. Effect of trapping agent on photocatalytic degradation of RhB (2×10^{-5} mol/L) under visible light irradiation ($\lambda > 400$ nm). (a) g-C_3N_4 (b) g-C_3N_4/ZnTcPc. [g-C_3N_4/ZnTcPc] = 0.1 g/L, [g-C_3N_4] = 0.1 g/L pH 9.

3.3. Mechanism and pathway

3.3.1. Mechanism

In order to demonstrate the mechanism for the photocatalytic degradation of RhB over g-C_3N_4 and g-C_3N_4/ZnTcPc, the scavengers BQ, KI and IPA were added to quench the possible active species $^{\bullet}O_2^-$, hole (h^+) and $^{\bullet}OH$, respectively [41–44]. As shown in Fig. 7a when BQ and IPA were added, the removal rate of RhB had no obvious decrease, implying that $^{\bullet}O_2^-$ and $^{\bullet}OH$ did not dominate the photocatalytic reaction with g-C_3N_4. However, the dramatic decline of RhB removal was achieved in the presence of KI, suggesting that h^+ was the main active species. This result is coincident with that obtained in the common g-C_3N_4 photocatalytic system [45]. Since no photocatalytic activity was achieved when ZnTcPc was present in the above activity test, we did not explore the influence of $^1O_2$ [30]. In the photocatalytic system with g-C_3N_4/ZnTcPc, there might be three active species during the degradation of RhB (Fig. 7b). As can been seen, h^+ is also the main active species in the g-C_3N_4/ZnTcPc catalytic system, simultaneously with the formation of $^{\bullet}O_2^-$ and $^{\bullet}OH$. The photocatalytic mechanism of g-C_3N_4 has been transformed from the main h^+ species to the synergistic effect of all the three active species when g-C_3N_4 was coupled with ZnTcPc. To further investigate the mechanism for the photocatalytic degradation of 4-CP, we investigated the effect of concentration of dissolved oxygen on photocatalytic degradation of 4-CP under visible light irradiation (Fig. S8). The photocatalytic performance of bubbling O_2 is better than that of no bubbling O_2 in the presence of ZnTcPc and g-C_3N_4/ZnTcPc. The increase of O_2 concentration might be beneficial to the formation of the oxygen free radicals ($^1O_2$, $^{\bullet}O_2^-$ and

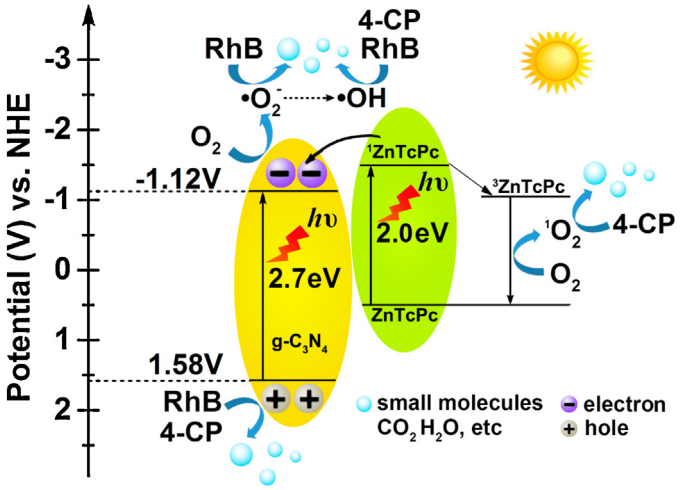

Fig. 8. Schematic diagram of electron–hole pairs separation and the possible reaction mechanism over g-C_3N_4/ZnTcPc photocatalyst under visible light irradiation (λ > 400 nm).

•OH). This can be inferred that the decrease of $^1O_2$ and $•O_2^-$ after bubbling O_2 could lead to the reduced amount of •OH. Furthermore, EPR spin-trapping technique was employed to investigate the current reaction mechanism (Figs. S9 and S10). As shown in Fig. S9, g-C_3N_4/ZnTcPc can produce the active species of •OH and $•O_2^-$. As for Fig. S10, it infers that the introduction of ZnTcPc makes g-C_3N_4/ZnTcPc generate the active species of $^1O_2$, which is consistent with the above results.

Accordingly, the photocatalytic mechanism for RhB and 4-CP degradation photocatalyzed by g-C_3N_4/ZnTcPc was proposed in Fig. 8. The photogenerated electron–hole pairs of g-C_3N_4 and ZnTcPc were excited simultaneously under visible light irradiation. $^1O_2$ is generated by interaction between ZnTcPc in excited triplet state and oxygen, and could effectively eliminate 4-CP. Since, the lowest unoccupied molecular orbital (LUMO) of ZnTcPc is higher than the conduction band (CB) of g-C_3N_4, the excited electrons on ZnTcPc could be easily injected to g-C_3N_4, making charge separation more efficient and reducing the probability of recombination. The formed h^+ on g-C_3N_4 has a critical role in the degradation of both RhB and 4-CP. Furthermore, the photogenerated electrons on the conduction band of g-C_3N_4 can further react with dissolved oxygen to form $•O_2^-$, which is capable for the degradation of RhB. Meanwhile, the one electron reduction or the disproportionation of $•O_2^-$ resulted in the formation of H_2O_2, which could react with the conduction band electron to produce •OH [46,47]. The formation of active species including $^1O_2$, $•O_2^-$ and •OH resulted in a significantly enhanced photocatalytic activity in the g-C_3N_4/ZnTcPc catalytic system under visible light irradiation.

Presently, the photocurrent is widely regarded as the most efficient evidence demonstrating the charge separation in the composite photocatalysts [48,49]. To give further evidence to support the mechanism given above, the photocurrent–time measurements were performed by the on-off cycles under a 671 nm laser and visible light (λ > 400 nm) irradiation. As shown in Fig. 9a, g-C_3N_4/ZnTcPc has a better response to a 671 nm laser than pure g-C_3N_4. The similar light source as the photocatalytic reaction was used in the transient photocurrent density response experiment (Fig. 9b). g-C_3N_4/ZnTcPc also shows higher current than pure g-C_3N_4 and ZnTcPc. It suggests that the photogenerated electron–hole pairs of g-C_3N_4/ZnTcPc are efficiently separated both under laser and visible light irradiation and have the lower electron–hole recombination rate.

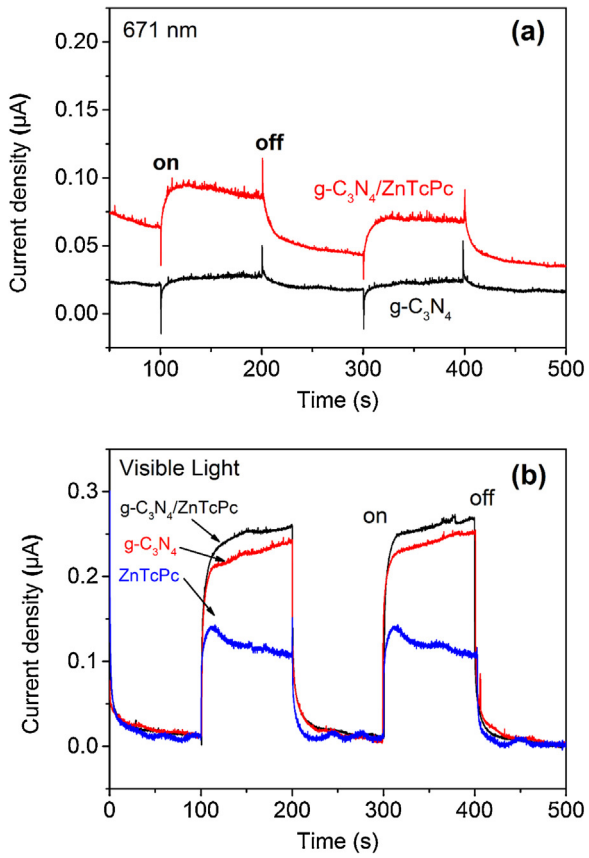

Fig. 9. The transient photocurrent density response of g-C_3N_4, ZnTcPc and g-C_3N_4/ZnTcPc photocatalysts electrodes with light on-off cycles under a 671 nm laser (a) and visible light (λ > 400 nm) irradiation (b). [Na_2SO_4] = 0.1 M.

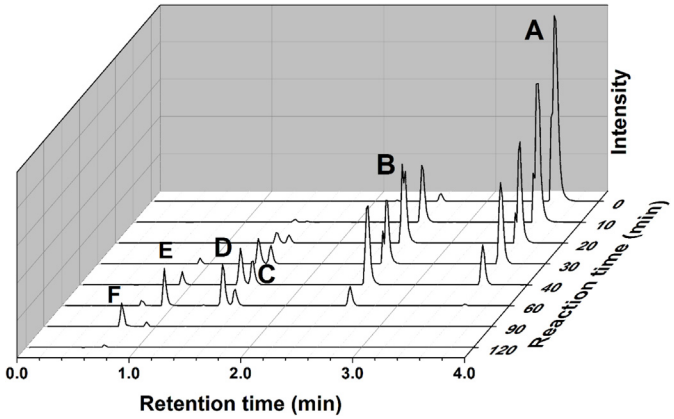

Fig. 10. Temporal UPLC spectra profiles during the photocatalytic degradation of RhB (2×10^{-5} mol/L) obtained from UPLC Synapt G2-S HDMS.

3.3.2. Degradation pathway

The degradation intermediates of RhB in the catalytic system based on g-C_3N_4/ZnTcPc were examined by UPLC Synapt G2-S HDMS in the both positive and negative ion mode at different irradiation intervals. Temporal UPLC spectra profiles during the photocatalytic degradation of RhB were shown in Fig. 10, the peak (A) of RhB gradually declined, while the peak (B) with a retention time of ~2.56 min, the peak (C) with a retention time of ~1.52 min, and the peak (D) with a retention time of ~1.41 min decreased after an initial increase. The peak (E) appeared after 30 min and disappeared after 120 min. After irradiation for 120 min, only the peak (F) was left. These results elucidated that the formation and

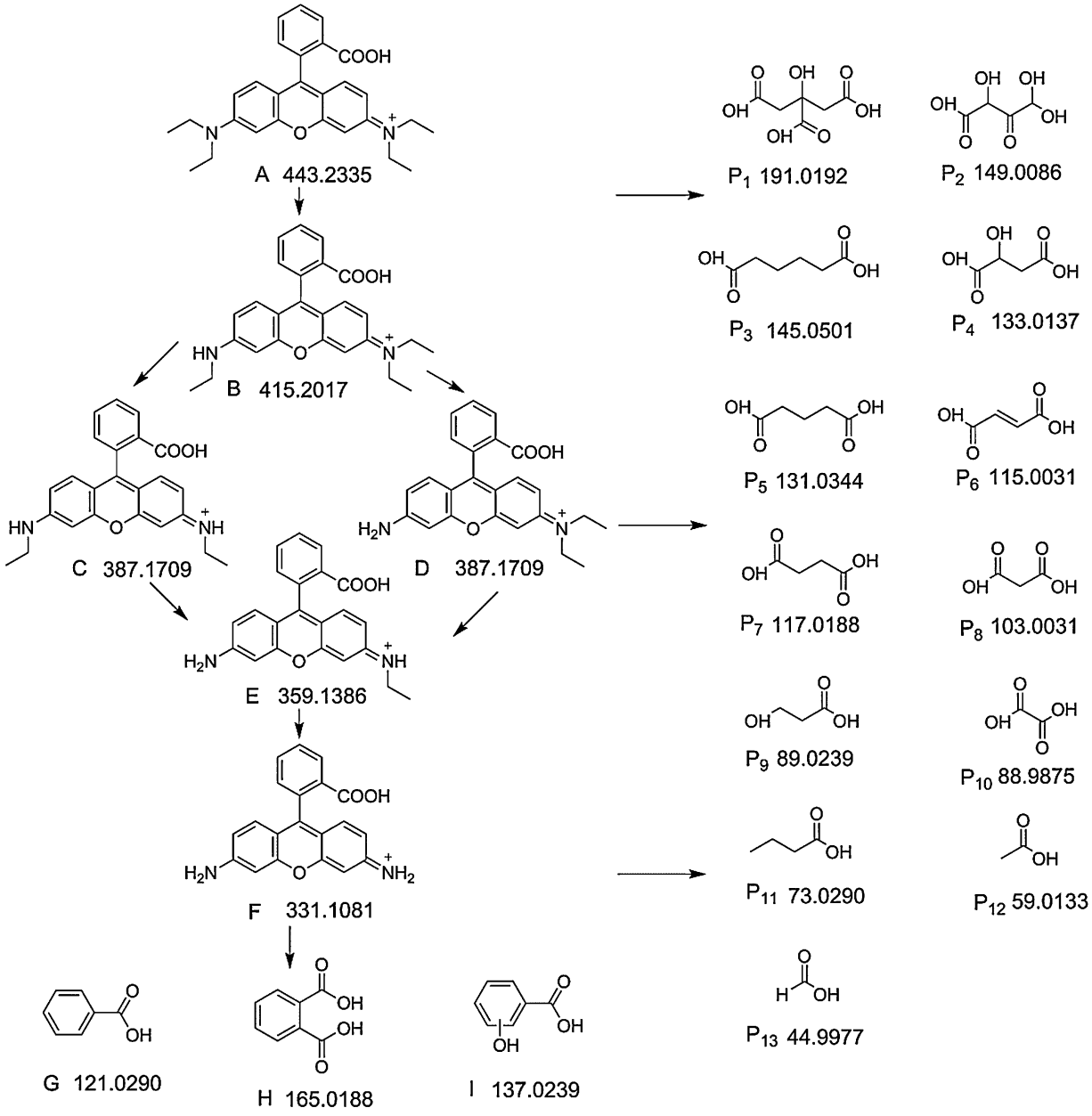

Fig. 11. Possible pathway for the photocatalytic degradation of RhB in the presence of g-C_3N_4/ZnTcPc (A–F were detected by UPLC Synapt G2-S HDMS in the positive ion mode, and G–I, P_1–P_{13} were detected in the negative ion mode.).

transformation of the intermediates and *N*-de-ethylation of RhB is a stepwise course. The five *N*-de-ethylated intermediates of RhB were evidently identified in the positive ion mode by UPLC Synapt G2-S HDMS, namely, *N*,*N*-diethyl-*N*′-ethylrhodamine (DER), *N*-ethyl-*N*′-ethylrhodamine (EER), *N*,*N*-diethylrhodamine (DR), N-ethylrhodamine (ER), and rhodamine (R), corresponding to peaks B–F, respectively. It is worth noting that when the solution is monitored at the *m*/*z* 387.1709 mode, two peaks (C and D) appeared in the chromatogram. Both of them are regarded to be the intermediates that possess two less ethyl groups relative to the RhB dye. DR is one of the isomers that lost two ethyl groups at the same side of RhB; the other one is formed by the removal of an ethyl group from each side of the RhB, noted as EER. EER species is expected to be eluted off the LC column after DR because of its weaker polarity [50]. The possible degradation pathway was shown in Fig. 11 and the degradation intermediates were listed in Tables S1 and S2. Besides the *N*-de-ethylated intermediates, some other intermediates can also be observed by UPLC Synapt G2-S HDMS in the negative ion mode. As shown in Fig. 11, three benzenoid removal intermediates (G–I), including benzoic acid, hydroxybenzoic acid, phthalic acid were identified. Finally, thirteen biodegradable small molecular acids (P_1–P_{13}) were obtained due to aromatic ring-opening oxidation.

4. Conclusion

A series of g-C_3N_4 coupled with ZnTcPc photocatalysts, g-C_3N_4/ZnTcPc, with enhanced visible light photocatalytic efficiency for the oxidation of RhB and 4-CP were prepared. The strong conjugate interaction between g-C_3N_4 and ZnTcPc played an important role in enhancing the photocatalytic activity of pure g-C_3N_4 and ZnTcPc, which was attributed to the electron transfer from the excited ZnTcPc to g-C_3N_4, resulting in the effective separation of photogenerated electron–hole pairs. Moreover, the photocat-

alytic activity of g-C_3N_4/ZnTcPc was higher than that of the simple mixture of g-C_3N_4 and ZnTcPc, and this system exhibited higher catalytic activity over a wide pH range due to the formation of active species including $^1O_2$, $^\bullet O_2^-$ and •OH. The pollutants were ultimately degraded into biodegradable small molecules. Therefore, this work provides a practical method in combining two visible light photocatalysts to expand their visible light absorption, and this synergistic photocatalytic mechanism provides useful insights to improve the performance of traditional photocatalysts.

Author contributions

The manuscript was written through contributions of all authors. All authors have given approval to the final version of the manuscript.

Competing interest

The authors declare no competing financial interest.

Acknowledgments

This work was supported by the National Natural Science Foundation of China (No. 51133006 and 51103133), Textile Vision Science & Education Fund, 521 Talent Project of ZSTU, and Zhejiang Provincial Natural Science Foundation of China (No. LY14E030013 and LY14E030015), and the Public Welfare Technology Application Research Project of Zhejiang Province (NO. 2015C33018).

Appendix A. Supplementary data

Supplementary data associated with this article can be found, in the online version, at http://dx.doi.org/10.1016/j.apcatb.2015.06.009

References

[1] Y. Ding, F. Yang, L. Zhu, N. Wang, H. Tang, Appl. Catal. B: Environ. 164 (2015) 151–158.
[2] Z. He, C. Sun, S. Yang, Y. Ding, H. He, Z. Wang, J. Hazard. Mater. 162 (2009) 1477–1486.
[3] J. Kim, J. Kim, Environ. Sci. Technol. 48 (2014) 13384–13391.
[4] A. Fujishima, Nature 238 (1972) 37–38.
[5] A.L. Linsebigler, G. Lu, J.T. Yates Jr, Chem. Rev. 95 (1995) 735–758.
[6] H. Fang, Y. Gao, G. Li, J. An, P.K. Wong, H. Fu, S. Yao, X. Nie, T. An, Environ. Sci. Technol. 47 (2013) 2704–2712.
[7] P. Li, Z. Wei, T. Wu, Q. Peng, Y. Li, J. Am. Chem. Soc. 133 (2011) 5660–5663.
[8] P. Raizada, P. Singh, A. Kumar, G. Sharma, B. Pare, S.B. Jonnalagadda, P. Thakur, Appl. Catal. A: Gen. 486 (2014) 159–169.
[9] Z. Yu, B. Yin, F. Qu, X. Wu, Chem. Eng. J. 258 (2014) 203–209.
[10] X. Dai, M. Xie, S. Meng, X. Fu, S. Chen, Appl. Catal. B: Environ. 158–159 (2014) 382–390.
[11] X. Wang, K. Maeda, A. Thomas, K. Takanabe, G. Xin, J.M. Carlsson, K. Domen, M. Antonietti, Nat. Mater. 8 (2009) 76–80.
[12] F. Goettmann, A. Fischer, M. Antonietti, A. Thomas, Angew. Chem. Int. Ed. 45 (2006) 4467–4471.
[13] S. Yan, S. Lv, Z. Li, Z. Zou, Dalton Trans. 39 (2010) 1488–1491.
[14] Y. Wang, J. Yao, H. Li, D. Su, M. Antonietti, J. Am. Chem. Soc. 133 (2011) 2362–2365.
[15] X. Wang, S. Blechert, M. Antonietti, ACS Catal. 2 (2012) 1596–1606.
[16] Y. Wang, X. Wang, M. Antonietti, Angew. Chem. Int. Ed. 51 (2012) 68–89.
[17] S. Cao, J. Yu, J. Phy. Chem. Lett. 5 (2014) 2101–2107.
[18] S. Zhang, J. Li, M. Zeng, G. Zhao, J. Xu, W. Hu, X. Wang, ACS Appl. Mater. Interfaces 5 (2013) 12735–12743.
[19] H. Li, J. Liu, W. Hou, N. Du, R. Zhang, X. Tao, Appl. Catal. B: Environ. 160–161 (2014) 89–97.
[20] S. Wang, D. Li, C. Sun, S. Yang, Y. Guan, H. He, Appl. Catal. B: Environ. 144 (2014) 885–892.
[21] W. Wang, J.C. Yu, D. Xia, P.K. Wong, Y. Li, Environ. Sci. Technol. 47 (2013) 8724–8732.
[22] J. Xu, G. Wang, J. Fan, B. Liu, S. Cao, J. Yu, J. Power Sources 274 (2015) 77–84.
[23] G. Pellegrino, G.G. Condorelli, F. De Rossi, T.M. Brown, F. Giovenale, C. Bongiorno, A. Alberti, Appl. Surf. Sci. 296 (2014) 69–78.
[24] E.L. Coitiño, A. Mella, G.I. Cárdenas-Jirón, J. Photochem. Photobiol. A: Chem. 294 (2014) 68–74.
[25] P. Zhao, L.-C. Xu, J.-W. Huang, K.-C. Zheng, B. Fu, H.-C. Yu, L.-N. Ji, Biophys. Chem. 135 (2008) 102–109.
[26] Z. Huang, B. Zheng, S. Zhu, Y. Yao, Y. Ye, W. Lu, W. Chen, Mater. Sci. Semicond. Process. 25 (2014) 148–152.
[27] Y. Yao, Z. Huang, B. Zheng, S. Zhu, W. Lu, W. Chen, H. Chen, Curr. Appl. Phys. 13 (2013) 1738–1742.
[28] W. Lu, C. Sun, Q. Lu, N. Li, D. Wu, Y. Yao, W. Chen, Sci. China Chem. 55 (2012) 1108–1114.
[29] C. Zhou, Y. Liu, X. Zhao, Inorg. Chim. Acta 425 (2015) 11–16.
[30] M. Gao, N. Li, W. Lu, W. Chen, Appl. Catal. B: Environ. 147 (2014) 805–812.
[31] F. Dong, L. Wu, Y. Sun, M. Fu, Z. Wu, S.C. Lee, J. Mater. Chem. 21 (2011) 15171.
[32] E. Fitzer, K.-H. Geigl, W. Hüttner, R. Weiss, Carbon 18 (1980) 389–393.
[33] J. Li, B. Shen, Z. Hong, B. Lin, B. Gao, Y. Chen, Chem. Commun. 48 (12) (2012) 017–12019.
[34] A. Thomas, A. Fischer, F. Goettmann, M. Antonietti, J.-O. Müller, R. Schlögl, J.M. Carlsson, J. Mater. Chem. 18 (2008) 4893–4908.
[35] J. Zhang, M. Zhang, G. Zhang, X. Wang, ACS Catal. 2 (2012) 940–948.
[36] K. Nilson, P. Palmgren, J. Åhlund, J. Schiessling, E. Göthelid, N. Mårtensson, C. Puglia, M. Göthelid, Surf. Sci. 602 (2008) 452–459.
[37] S. Yang, Y. Gong, J. Zhang, L. Zhan, L. Ma, Z. Fang, R. Vajtai, X. Wang, P.M. Ajayan, Adv. Mater. 25 (2013) 2452–2456.
[38] Y.-P. Zhu, M. Li, Y.-L. Liu, T.-Z. Ren, Z.-Y. Yuan, J. Phys. Chem. C 118 (2014) 10963–10971.
[39] S. Chen, Y. Liu, Chemosphere 67 (2007) 1010–1017.
[40] A.K. Roy Choudhury, Textile Preparation And Dyeing, Science Publishers, Enfield, NH, 2006, pp. 62–63.
[41] W. Li, D. Li, Y. Lin, P. Wang, W. Chen, X. Fu, Y. Shao, J. Phys. Chem. C 116 (2012) 3552–3560.
[42] J. Cao, B. Luo, H. Lin, B. Xu, S. Chen, Appl. Catal. B: Environ. 111 (2012) 288–296.
[43] C. Chang, L. Zhu, S. Wang, X. Chu, L. Yue, ACS Appl. Mater. Interfaces 6 (2014) 5083–5093.
[44] L. Mohapatra, K. Parida, M. Satpathy, J. Phys. Chem. C 116 (2012) 13063–13070.
[45] S.C. Yan, Z.S. Li, Z.G. Zou, Langmuir 26 (2010) 3894–3901.
[46] C. Chen, W. Ma, J. Zhao, Chem. Soc. Rev. 39 (2010) 4206–4219.
[47] S. Ge, L. Zhang, Environ. Sci. Technol. 45 (2011) 3027–3033.
[48] Q. Xiang, J. Yu, M. Jaroniec, J. Phys. Chem. C 115 (2011) 7355–7363.
[49] M. Kong, Y. Li, X. Chen, T. Tian, P. Fang, F. Zheng, X. Zhao, J. Am. Chem. Soc. 133 (2011) 16414–16417.
[50] K. Yu, S. Yang, H. He, C. Sun, C. Gu, Y. Ju, J. Phys. Chem. A 113 (2009) 10024–10032.